A Vision-based Semi-autonomous Impedance Control Method in Teleoperation

Msc. Thesis

Y. Huang

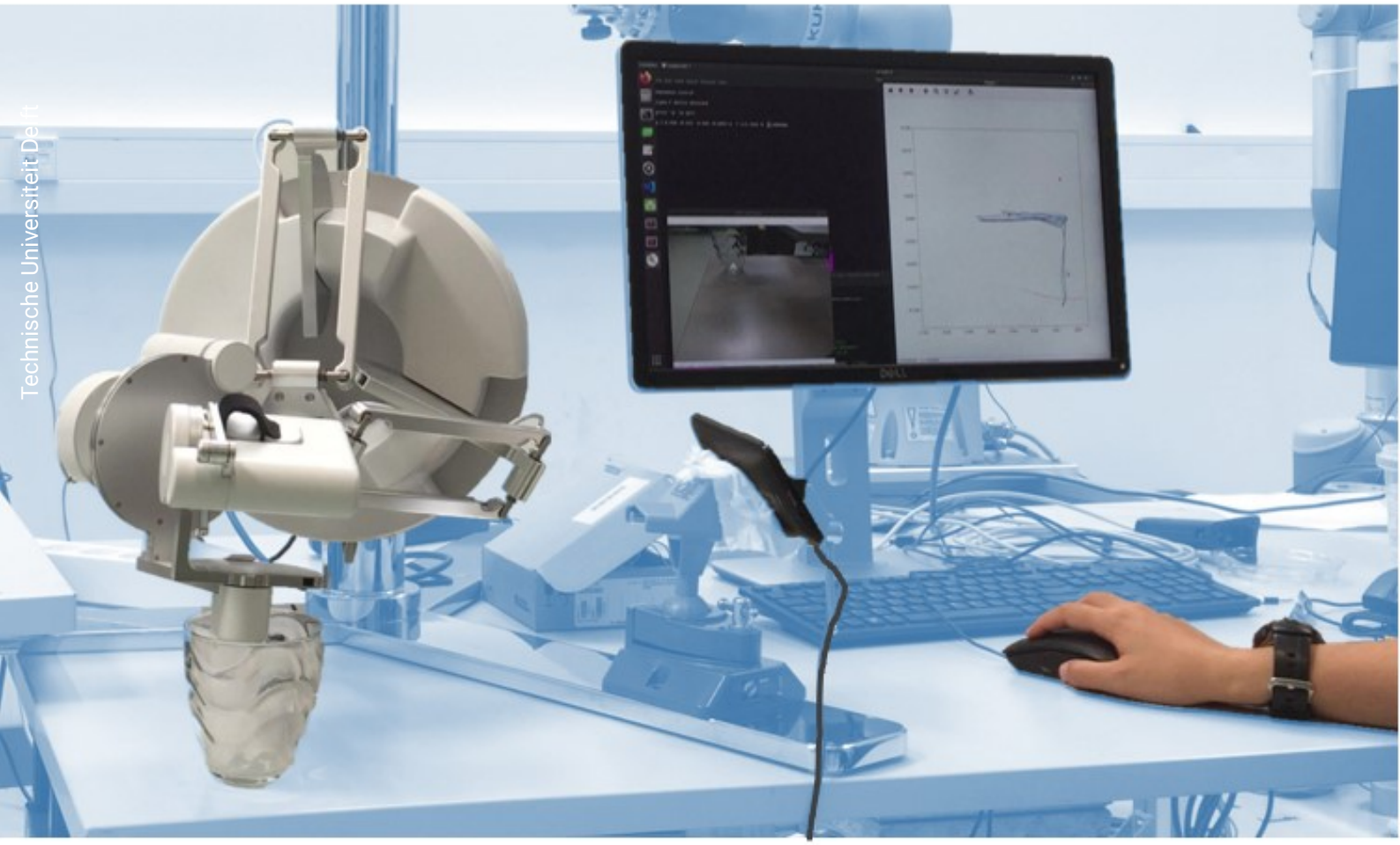

TU Delft

A Vision-based Semi-autonomous Impedance Control Method in Teleoperation

Msc. Thesis

by

Y. Huang

to obtain the degree of Master of Science
at the Delft University of Technology,
to be defended publicly on Monday August 24th, 2020 at 10:00 AM.

Student number:	4799100	
Project duration:	February 11, 2019 – August 24, 2020	
Thesis committee:	Prof. dr. ir. D.A. Abbink,	TU Delft, supervisor
	Dr. L. Peternel,	TU Delft, supervisor
	Dr. ing. J. Kober,	TU Delft, external member
	Dr. W. Roozing,	University of Twente, external member

This thesis is confidential and cannot be made public until August 24, 2021.

TU Delft

Preface

This master thesis is the final step of my master's program in Mechanical Engineering at the Delft University of Technology. In this 6-month thesis project, I developed a novel vision-based semi-autonomous impedance control method, which can partially offload the impedance control task from humans, and validated it on a teleopration setup.

The first part of the report is a journal paper that summarizes the main results and conclusions of the project work. The second part consists of appendices that provide more detailed descriptions of the method implementation and other information about the experiments conducted in the thesis project.

I would like to thank everyone who helped and supported me during this project. In particular, I wish to express my gratitude to my supervisors, Professor David Abbink and Professor Luka Peternel for their excellent supervision. David provided guidance from a higher level that helped steer the project in the right direction, he challenged me with questions and encouraged me to do the right thing even if that means choosing the tougher path. Luka provided support and advice every step of the way, he was always willing to help with problems I ran into during my research or writing, his persistent help was crucial to the creation of this thesis project.

I would also like to thank my friends, Andrea, Chih-Yu, and Kushal, for reviewing my paper and giving me valuable comments.

Finally, I wish to acknowledge the unconditional love and support from my parents, Wen-Chang and Chao-Jung, and my sister, Yu-Ching. I would not have been able to complete this journey without them. Thank you.

Y. Huang
Delft, August 2020

Contents

A Vision-based Semi-autonomous Impedance Control Method in Teleoperation

Student: Yu-Chih Huang(4799100)
Supervised by Prof. dr. ir. David Abbink
and Dr. Luka Peternel

***Abstract*—Teleoperation of a robot is often necessary when the remote site is not safe for humans. Moreover, to interact with dynamic environments safely, a teleoperation method called teleimpedance, which allows the human operator to control the impedance of the robot, is used. The main drawback of this method is that the human workload may increase. This could be tackled by using autonomous impedance controllers to relieve the human operator from this added workload. However, most of the existing autonomous impedance controllers require physical contact before adjusting to unexpected environmental changes. This study presents a novel semi-autonomous impedance control method that includes a vision-based autonomous impedance controller and a voice-based impedance control interface. The first element allows the robot to adjust to the environment before contact, whereas the second element allows the human operator to interact with the impedance controller when the vision-based autonomy is performing poorly or not sufficient under the environment. The method has four modalities: (i) Perturbation rejection mode, (ii) Object property detection mode, (iii) Verbal confirmation mode, (iv) Voice control mode. To provide a proof-of-concept of the proposed method, experiments were performed on a teleoperation setup that uses a Force Dimension Sigma.7 as the slave robot, a computer mouse as the master device, and a camera device. The proposed method was analyzed with a position tracking task and contact establishing task, where changing impedance can be crucial and beneficial.**

***Index Terms*—Impedance, Teleoperation, Vision-based, Semi-autonomous.**

I. Introduction

Tasks in hazardous or remote environments often require robots to perform them because such environments are unsafe or hard to reach for humans. Moreover, some of these tasks involve the interaction with dynamic environments, which could be too complex for fully autonomous robots to handle with the current artificial intelligence (AI) capacity. To make robots able to interact with dynamic environments, human adaptability and cognitive capabilities are introduced to robot systems through human-in-the-loop control. One common way to achieve this is teleoperation [1].

In classical teleoperation, the human operator can control the motion of the slave robot remotely through a master device. However, the fact that it focuses only on position control can result in the robot damaging the environment with high interaction forces or causing unstable interactions when establishing contact with an environment. Unlike robots, humans can instinctively adjust their neuromuscular impedance according to changes in the environment [2], [3]. In order to address the lack of ability to interact with dynamic environments in classical teleoperation, a concept called teleimpedance that allows the human operator to control the impedance of the robot was developed in the past years [4], [5].

Teleimpedance includes an additional channel of impedance command to the classical teleoperation setup, which can be realized with an interface. Although using teleimpedance allows the robot to interact with dynamic environments, it also comes with some drawbacks. The state-of-the-art interfaces in teleimpedance, such as the button interface [6] and the Electromyography (EMG) interfaces [7]–[9], have certain shortcomings. For the button interface, the human operator must press the button with one finger, thus losing 1 Degree of Freedom (DoF). Moreoever, the EMG interface needs a setup of electrodes to measure the EMG signals, and requires time-consuming calibrations.

Another drawback of using teleimpedance is that the setup may significantly increase the workload of the human operator compared to a classical teleoperation setup. Therefore, if the human operator's workload can be partially relieved, their overall performance might improve because they only have to focus on motion control instead of both tasks. The fatigue of the human operator would also not accumulate as fast. Autonomous impedance controllers and shared control methods can be introduced to the teleportation system to offload the impedance control task from the human operator.

There are numerous studies dedicated to developing autonomous impedance controllers, but only a few can be used in teleoperation. Autonomous impedance controllers developed with learning methods, such as reinforcement learning [10] or learning from demonstration [11]–[13] cannot be used in teleoperation systems because the impedance values are learned with a fixed trajectory. This is not compatible with teleoperation because human operators need to change the trajectory rapidly while the impedance is adjusting. One type of impedance controllers that is suitable for teleoperation systems is an adaptive impedance controller. Within this category, research has been conducted to develop controllers that mimic human behaviour [14], or that adjust the impedance relying on information of the environment acquired through sensors [15]–[17]. However, most of them adjust the impedance only after interaction with the environment has been established, which might not be an optimal approach in situations where the environment is unstable or fragile. To solve this problem, the appropriate change in impedance prior to contact could be

Online resource available at: https://www.youtube.com/playlist?list=PLyVZusC3uqby-yTSGuCyibykTLqpMdVae

estimated by visual feedback.

In addition to an autonomous impedance controller, a shared control method is needed to offload the impedance control task. Many studies investigated the shared control method in teleoperation with different purposes, such as teaching with shared control [18]–[20], assistive shared control [21]–[23], or collaborative shared control [24]. However, most of these studies focus mainly on motion control, and only a few considered impedance control [8], [16]. Although in the studies of [8] and [16], impedance control was considered, both studies do not have vision-based impedance capability and requires interactions with the environment to make adjustments in their impedance.

This research aims to develop a vision-based semi-autonomous impedance control method that can adjust the impedance of the robot prior to contact, in order to fill the gap in research and address the disadvantage of autonomous impedance controllers that require physical contacts to adjust. The method is inspired by how humans use vision to adjust their postural impedance before interacting with the environment.

The proposed method, which includes a vision-based autonomous impedance controller and a voice-based impedance control interface, has four modalities with different levels of autonomy. The two fully autonomous modes are incorporated within the vision-based autonomous impedance controller. The controller uses collision detection to predict incoming perturbations in the perturbation rejection mode and uses object property detection algorithms to acquire environment information without physical contact in the object property detection mode. However, because current detection algorithms do not have perfect accuracy yet, the voice-based impedance control interface is included to allow the human operator to interact with the vision-based autonomous impedance controller and override its decisions if necessary. The voice-based impedance control interface also contains two modes, where the verbal confirmation mode shares the impedance control between the operator and the controller, and the voice control mode takes over the impedance control entirely.

This study introduces a novel vision-based semi-autonomous impedance control method in teleoperation and conducts proof-of-concept validation experiments. The experiments were performed on a teleoperation setup with a Force Dimension Sigma.7 haptic device as the slave robot, a computer mouse as the master device, and a camera device for visual feedback. The experiments consist of two tasks that demonstrate the performance of each modality of the proposed method: rejecting external perturbations in a position tracking task and establishing contact with different objects.

A description of the impedance control of the robot used in this study is given in section II. The two elements in the proposed impedance control method, the vision-based autonomous impedance controller and the voice-based impedance control interface, are introduced in section III and IV, respectively. This is followed by the proof-of-concept experiments in section V, the discussion of the results in section VI, and conclusions in section VII.

II. Impedance control of the robot

A. General Control Scheme

The block scheme of the proposed vision-based semi-autonomous impedance control method is shown in Fig. 1. The human operator controls the motion of the robot through a master device with optional force feedback on the master device (see Appendix A.1). The method has four modalities: (i) Perturbation rejection mode; (ii) Object property detection mode; (iii) Verbal confirmation mode; (iv) Voice control mode. The two autonomous modes (mode i, ii) are part of the vision-based autonomous impedance controller, where the controller processes the camera feed with vision algorithms and sends the proper impedance command to the robot. The impedance is performed by the robot using the Cartesian impedance control method. The physical interactions between the slave robot and the environment are shown in Fig. 1, where the robot exerts a force $\boldsymbol{F}_s$ on the environment, and the environment exerts a force $\boldsymbol{F}_{ext}$ on the robot. During the interactions, the human operator can assess the situation through visual feedback and, if needed, activate the voice-based impedance control interface to override the robot impedance value with the verbal confirmation mode (mode iii) or the voice control mode (mode iv).

B. Robot Stiffness Control

The Cartesian impedance control method was used on the Sigma.7 robot which has 7 DOFs where 6 DoFs are from the rotation and translation of the robot, and 1 DoF is from the gripping button on the robot. However, the proposed method in this study focuses only on controlling the stiffness and damping coefficient in translation axes of the robot end-effector so the following derivation will only consider 3 DoFs instead of 7 DoFs, which excludes the degrees of freedom for rotation (3 DoFs) and the gripping button (1 DoF).

The robot's physical interactions are controlled by a Cartesian impedance controller defined as:

$$\boldsymbol{f} = \boldsymbol{D}(\dot{\boldsymbol{x}}_d - \dot{\boldsymbol{x}}_a) + \boldsymbol{K}(\boldsymbol{x}_d - \boldsymbol{x}_a) \tag{1}$$

where $\boldsymbol{f} \in \mathbb{R}^3$ is the endpoint force exerted by the robot on the environment, $\boldsymbol{x}_d \in \mathbb{R}^3$ and $\boldsymbol{x}_a \in \mathbb{R}^3$ are the desired and the actual end-effector position of the robot. $\boldsymbol{K} \in \mathbb{R}^{3x3}$ is the Cartesian stiffness matrix and $\boldsymbol{D} \in \mathbb{R}^{3x3}$ is the Cartesian damping matrix. The stiffness matrix $\boldsymbol{K}$ is given by either the autonomous impedance controller or the human operator as $\text{diag}\{\boldsymbol{k}\}$ where $\boldsymbol{k} = [k_x \; k_y \; k_z]$ [25]. The damping matrix $\boldsymbol{D}$ was designed based on the stiffness matrix $\boldsymbol{K}$ at each time-step:

$$\boldsymbol{D} = 2\boldsymbol{D}_\xi\sqrt{\boldsymbol{K}} \tag{2}$$

where $\boldsymbol{D}_\xi \in \mathbb{R}^{3x3}$ is a diagonal matrix that contains the damping factors, which were set to 0.7 for critical damping in this study.

A robot model of n-flexible joints [26] is considered in joint space because the robot is controlled by actuating each joint with the desired torque:

$$\boldsymbol{M}(\boldsymbol{q})\ddot{\boldsymbol{q}} + \boldsymbol{C}(\dot{\boldsymbol{q}})\dot{\boldsymbol{q}} + \boldsymbol{g}(\boldsymbol{q}) = \boldsymbol{\tau} + \boldsymbol{\tau}_{ext} \tag{3}$$

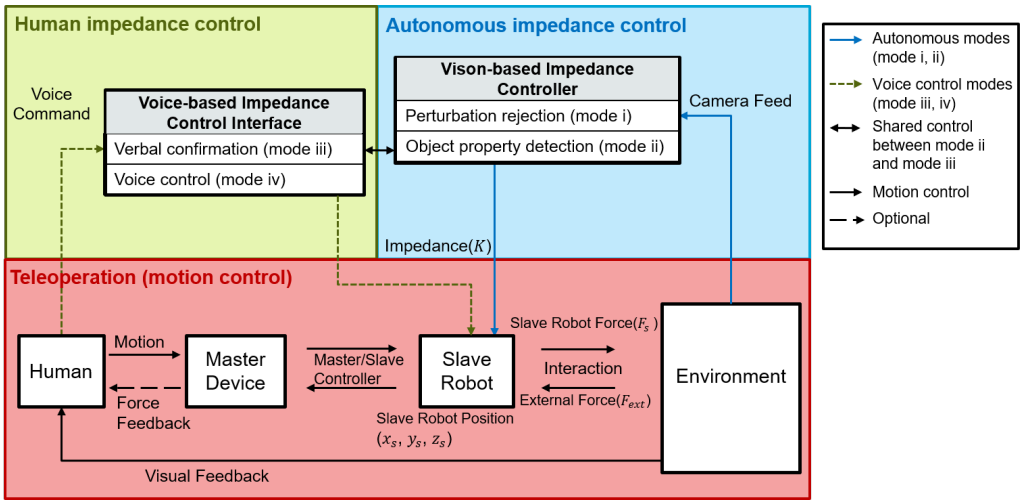

Fig. 1. Block diagram of the vision-based semi-autonomous impedance control method. The bottom block (red) is the teleoperation framework for motion control. The upper half is the impedance control loop. The autonomous impedance control block (blue) contains the vision-based autonomous impedance controller with the perturbation rejection mode (mode i) and the object property detection mode (mode ii). The human impedance control block (green) contains the voice-based impedance control interface with the verbal confirmation mode (mode iii) and voice control mode (mode iv).

where $\boldsymbol{\tau} \in \mathbb{R}^3$ is a vector of robot joint torques, $\boldsymbol{q} \in \mathbb{R}^3$ is a vector of robot joint angles, $\boldsymbol{M} \in \mathbb{R}^{3x3}$ is the robot mass matrix, $\boldsymbol{C} \in \mathbb{R}^{3x3}$ is the Coriolis and centrifugal matrix, and $\boldsymbol{g} \in \mathbb{R}^3$ is the gravity vector.

The desired interaction force $\boldsymbol{f}$ can be mapped into the torque controlled scheme with the Jacobian matrix of the robot $\boldsymbol{J}$, and the torque input of the robot can be derived by:

$$\boldsymbol{\tau} = \boldsymbol{M}(\boldsymbol{q})\ddot{\boldsymbol{q}} + \boldsymbol{C}(\dot{\boldsymbol{q}})\dot{\boldsymbol{q}} + \boldsymbol{g}(\boldsymbol{q}) + \boldsymbol{J}^T(\boldsymbol{q})\boldsymbol{f} \tag{4}$$

where $\boldsymbol{J} \in \mathbb{R}^{3x3}$ is the Sigma.7 Jacobian matrix.

III. Vision-based Autonomous Impedance Controller

A. Perturbation Rejection Mode

1) Design Concept and Implementation: It is important for robots to follow the trajectory closely in a position tracking task if slight position errors could lead to unstable movements or damage the environment. For example, in a drilling task, the robot should hold its position perpendicular to the drilling direction under external perturbations to minimize the damage on the environment. To reject perturbations, the robot needs to increase its stiffness when perturbations are detected. The proposed perturbation rejection mode detects incoming perturbations through vision and increases the impedance beforehand to minimize position errors.

The advantage of the proposed perturbation rejection mode is that it does not require contact to adjust the impedance and can do so before any interaction unlike most of the existing autonomous impedance controllers mentioned in section I.

In order to detect perturbations with vision, a motion detection algorithm and a tracking algorithm are integrated (see Appendix A.2). The motion detection algorithm is used to detect any unknown objects that are moving within the camera view, and the object tracking algorithm is used to track the position of the robot. A perturbation is identified when the minimum distance between the detected motion and the robot is less than a defined safe distance. The robot will then increase its stiffness from a relatively low impedance $\boldsymbol{K}_L$ to high impedance $\boldsymbol{K}_H$ when perturbations are detected.

The algorithm is implemented using 2D vision since the objective of the design concept is to demonstrate the behaviour of reacting prior to making contact with the environment and before position tracking errors occur. However, other 3D collision detection vision algorithms could also be integrated into this impedance control method. In short, the key of the concept is to switch from relative low impedance $\boldsymbol{K}_L$ to high impedance $\boldsymbol{K}_H$ when the vision algorithms detect perturbations.

2) Design Evaluation: A position tracking experiment was conducted in simulation to compare the vision-based impedance controller with sensor-based impedance controllers. This approach is selected in order to generate the same perturbations, which would be hard to achieve in the real world.

We conducted the simulation with only one dimension (x-axis) for simplicity so we will refer to the impedance coefficients in robot impedance control as k and c, instead of the matrices $\boldsymbol{K}$ and $\boldsymbol{D}$ in this section. The sensor-based impedance controllers used in the simulation can be categorized into two types according to the sensor used, as shown in Table I.

To better standardize the comparison between vision-based controller and the two different types of sensor-based controllers, a position perturbation and a force perturbation were simulated to make the process repeatable (see Appendix B). To compare the vision-based controller with the position sensor-based controller group, a collision between an object and the robot arm was simulated to generate position perturbations. An impact force perturbation was simulated to compare the vision-based controller with the force sensor-based controller group.

TABLE I
A VISION-BASED AND SENSOR-BASED CONTROLLER SUMMARY

Controller	Impedance Value
Vision-based *(Perturbation detection)*	$k_L \rightarrow k_H$, if perturbation detected
Position sensor-based *(Function of position error)*	$k = k_L + \alpha(x_d - x)^2$ $\alpha \geq 0$ is a constant
Position sensor-based *(position error threshold, $e_{p,th}$, switching)*	$k = \begin{cases} k_L & \text{if } \lvert(x_d - x)\rvert < e_{p,th} \\ k_H & \text{if } \lvert(x_d - x)\rvert \geq e_{p,th} \end{cases}$
Force sensor-based *(Function of external force)*	$k = k_L + \beta {F_{ext}}^2$ $\beta \geq 0$ is a constant
Force sensor-based *(external force threshold, $e_{f,th}$, switching)*	$k = \begin{cases} k_L & \text{if } \lvert F_{ext}\rvert < e_{f,th} \\ k_H & \text{if } \lvert F_{ext}\rvert \geq e_{f,th} \end{cases}$

The desired position of the robot x_d is set to 0, so the reaction force of the robot with impedance control is calculated as:

$$F = -kx - c\dot{x} \tag{5}$$

where k is the stiffness of the robot, c is the damping coefficient, which equals to $2 * 0.7\sqrt{k}$, and x is the position of the robot, which also equals to the displacement from the desired position x_d since it is 0.

The system is considered to act as a spring-mass-damper system with the robot under impedance control, and the perturbations are the external forces exerted on the system. The robot positions were calculated by solving the following differential equation:

$$\ddot{x} == \frac{c}{m}\dot{x} - \frac{k}{m}x + \frac{F_{ext}}{m} \tag{6}$$

where x is the position of the robot. m is the total mass of the robot and the object, if it is a collision perturbation. Otherwise, m is the mass of the robot. F_{ext} is the external forces exerted on the system by perturbations. k is the stiffness of the robot, which is commanded by the impedance controller, and c is the damping coefficient which equals to $2 * 0.7\sqrt{k}$.

The results of the robot under the object collision perturbation show that the vision-based controller has a maximum position error of 0.063m, the position sensor-based controller (*function of position error*) has a maximum position error of 0.069m, and the position sensor-based controller (*position error threshold switching*) has a maximum position error of 0.088m. Moreover, under the impact force perturbation, the vision-based controller has a maximum position error of 0.05m, the force sensor-based controller (*function of external force*) has a maximum position error of 0.058m, and the force sensor-based controller (*external force threshold switching*) has a maximum position error of 0.091m. Under both perturbations, the vision-based controller had the least maximum position error among the other controllers, as shown in Fig. 2.

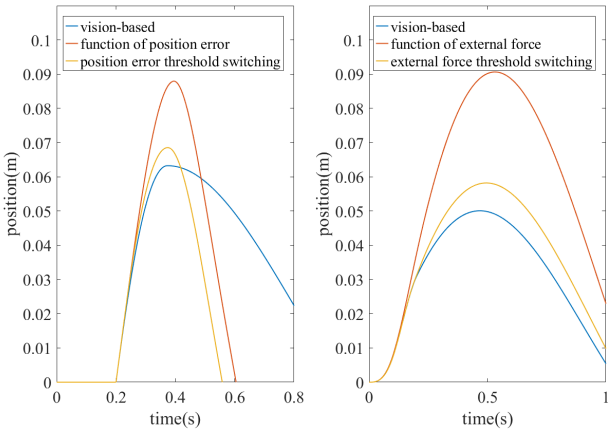

Fig. 2. Design evaluation of the perturbation rejection mode (mode i). The graph on the left shows the position of the robot controlled with the vision-based and the position sensor-based controllers under object collision perturbation. The graph on the right shows the position of the robot controlled with the vision-based and the force sensor-based controllers under impact force perturbation

B. Object Property Detection Mode

1) Design Concept and Implementation: Humans often use their experience along with visual cues to estimate the property of an object, and adjust their neuromuscular impedance to interact with the object. Inspired by this behaviour, the object property detection mode was designed to adjust the impedance according to the detected material. To make this possible, the relation between the material properties and the impedance has to be established.

The main two databases that were used in known studies on material recognition algorithms are the Flickr Material Database (FMD) and the Materials in Context Database (MINC). FMD was introduced in [27], the database has 10 categories with 100 samples in each category. MINC was introduced in [28], the database contains 23 categories with at least 14000 patches in each category. 10 materials (Glass, Leather, Metal, Paper, Plastic, Stone, Concrete, Wood, Ceramic, Rubber) were chosen from the databases and categorized into groups by their properties: elasticity and fragility (see Appendix C).

The results are shown in Table II. The chosen materials were categorized into three groups: "Rigid, Fragile", "Rigid, Not Fragile", "Elastic, Not Fragile", each group has a corresponding impedance value for better interaction performance. For example, if the material is in the "Rigid, Fragile" group then the robot should have a low impedance value for compliant interactions so that the robot will not damage the object, and if the material is in the "Elastic, Not Fragile" group, the robot should have a higher impedance so that the damping matrix would be higher to stabilize the interaction.

The developed relation between the material and the impedance was integrated into an object detection algorithm (see Appendix A.2). Ideally, the object property detection algorithm should be a material recognition algorithm instead of an object detection algorithm. However, the material recognition algorithms are not as widely available as object detection algorithms. Since this study did not focus on vision and visual recognition itself but rather on impedance control method that makes decision based on the vision output, an object detection algorithm (YOLOv3) [29] that can be easily implemented

TABLE II
A MATERIAL PROPERTY CATEGORIZATION TABLE

Material	Elasticity	Fragility
Glass	Rigid	Fragile
Leather	Elastic	Not Fragile
Metal	Rigid	Not Fragile
Paper	Rigid	Fragile
Plastic	Rigid	Not Fragile
Concrete	Rigid	Fragile
Stone	Rigid	Not Fragile
Wood	Rigid	Not Fragile
Ceramic (Engineering)	Rigid	Not Fragile
Rubber	Elastic	Not Fragile

was used. The algorithm output was adjusted into a type of material to make the method work smoothly for demonstration. Also note that the material recognition databases were taken as a reference when selecting the materials to analyze their properties and select corresponding impedance values, so it is still possible to implement material recognition algorithms in future work.

2) Design Evaluation: In the object property detection mode, the robot would change the impedance autonomously when the algorithm detects a material. In this case, the human operator only has to focus on the motion control of the robot. However, the detection algorithms can sometimes have low detection accuracy. Moreover, the impedance can only be changed discretely by switching between predefined impedance values, which might be insufficient if the task requires dynamic impedance changes. We improved the downfalls of the object property detection mode by having human input to correct the detection results or control the impedance dynamically.

IV. VOICE-BASED IMPEDANCE CONTROL INTERFACE

A. Verbal Confirmation Mode

1) Design Concept and Implementation: To deal with situations where the detection algorithm might not be accurate, a verbal command function was implemented in the verbal confirmation mode. It is activated when the confidence score of the detection result is lower than a predefined threshold. The robot will then announce the detected material, and the human operator is required to either confirm the detection results by saying "yes" or override the results by saying the correct material. This mode allows the human operator to partly offload the impedance control task to the robot, but can still have control when the robot is not so confident.

2) Design Evaluation: The object property detection mode and the verbal confirmation mode both have the same drawback, which is the impedance values can only be switched discretely between the predefined impedance values and cannot have impedance values in between or make small adjustments. This might be sufficient when the robot is approaching the object and establishing contact with different materials, except when it comes to executing an interactive task after the contact is established where the human operator would need to change the impedance continuously instead of switching discretely.

B. Voice Control Mode

1) Design Concept and Implementation: The voice control mode gives the human operator the ability to adjust the impedance value dynamically hands-free. This is done by analyzing the nominal frequencies of the audio data. The voice control mode can be activated by making a high pitch tone for 2-3 seconds. Once it is activated, the impedance control is assigned entirely to the human operator. The human operator can then adjust the impedance by making a high/low pitch tone.

The voice control mode changes the impedance value with a fixed speed determined by the set increment size and sample time. It processes the audio data in each loop to adjust the impedance as follow:

1) Receive audio data from the microphone.
2) Perform fast Fourier transform (FFT) on the audio data.
3) Get the top 3 nominal frequency signals, f_1, f_2, f_3 (large to small amplitude).
4) Calculate the average amplitude of f_1, f_2, f_3.
5) If the average amplitude is less than a noise threshold, then no impedance changes will be made. Otherwise, the voice command frequency f_c will be calculated to best represent the current tone: $f_c = \frac{3f_1+2f_2+f_3}{6}$.
6) If f_c is higher than the threshold frequency f_{th}, the impedance k increases by a increment size. On the contrary, the impedance k decreases by a increment size.

2) Design Evaluation: : An impedance profile following experiment on a graphic user interface (GUI) was performed to evaluate the control performance of the voice control mode (see Appendix D).

The user was asked to follow the given impedance profiles, which are a profile with step changes in impedance and a sine wave profile, using the voice control interface in this experiment. The impedance profile that contains step changes of impedance is an imitation of the real-world application, and the sine wave profile is used to evaluate the dynamic nature of this interface. The results in Fig. 3 show that the impedance increases when $f_c \geq f_{th}$, and decreases when $f_c < f_{th}$. Also, a dropping behaviour in the high voice command frequency can be seen compared to the low voice command frequency in the top graphs of Fig. 3. This indicates that it is harder for the user to maintain a high pitch tone than a low pitch tone. The commanded impedance k in the bottom graph of Fig. 3a shows that the impedance increased 150N/m within 1.1s and decreased 100N/m in 0.7s with a fixed slope. This is because the speed of changing in impedance is determined by the set increment size and the sample time. From the result shown in Fig 3b, the following performance could be evaluated with the impedance error k_{err}, which is defined as $|k_d - k|$. The mean value of k_{err} is 15.33 N/m and the maximum value of k_{err} is 45.58 N/m. Both values can be corrected in 4-10 sample time which means that the method follows the sine wave impedance profile closely.

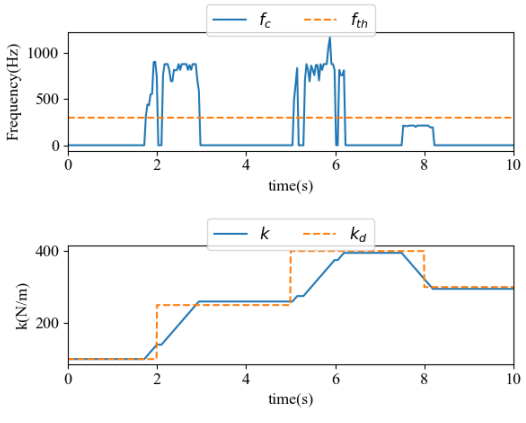

(a) Step change

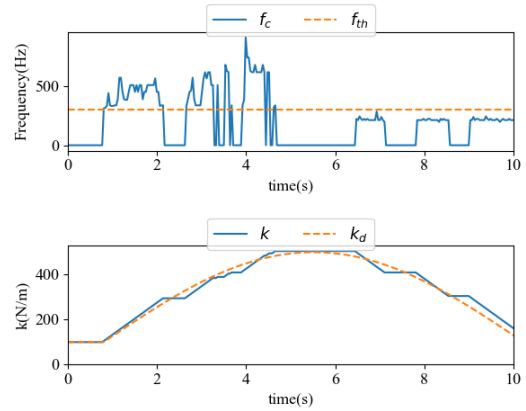

(b) Sine wave

Fig. 3. Design evaluation of the voice control mode (mode iv). The top graphs show the voice command frequency f_c and the threshold frequency f_{th}. The bottom graphs show the desired impedance profile k_d and the impedance commanded by the user k. (a) shows the step changes impedance profile following performance (b) shows the sine wave impedance profile following performance. (increment size: $\pm$5N/m, sample time: 0.035s).

V. Experiments

Proof-of-concept experiments were performed on a tele-operation setup that includes the Force Dimension Sigma.7 (7 DoF), a computer mouse (2 DoF), and a camera device (see Appendix A) to demonstrate the proposed vision-based semi-autonomous impedance control method in real-world applications (see Fig. 4). The computer mouse is the master device that controls the y-z plane motion of the Sigma.7, and the proposed method processes the camera feed captured by the camera device and sends the impedance value to the Sigma.7. The experiments involved two tasks, a position tracking task and a contact establishing task, where changing the impedance of the robot could be crucial or beneficial.

In all the experiments, there was no rotation with respect to the robot base frame in the impedance command matrix $\boldsymbol{K}$ and the proposed method commands the same impedance value for all axes in Cartesian space. Therefore, $\boldsymbol{K}$ was diagonal and had the same impedance value in all three axes. From now on, we will only simply describe and plot $\boldsymbol{K}$ as one value that represents the impedance in all three Cartesian axes.

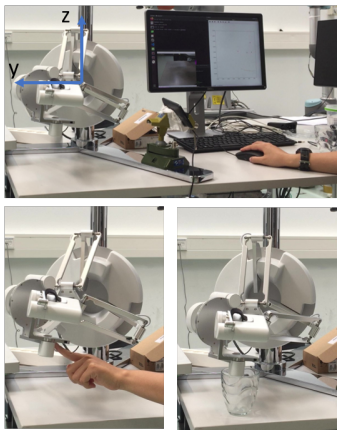

Fig. 4. Photos from the experiments. The photo on the top shows the human operator controlling the slave robot through the master device (computer mouse). The photo on the bottom left shows the position tracking experiment. The human assistant applies physical perturbations on the end-effector of the robot. The photo on the bottom right shows the contact establishing experiment. The human operator controls the robot to approach the object. The robot base frame orientation is illustrated by the blue arrows for y-axis and z-axis. The x-axis follows the right-handed coordinate system.

The first task was a position tracking task, the goal was to control the robot to hold its position while undertaking external perturbations. Ideally, the robot should be compliant to avoid large interaction forces that might damage the robot if possible. However, in some cases, where small position errors could lead to unstable interactions such as drilling, the priority of the task is to minimize position error caused by perturbations while following a reference trajectory, the robot's impedance had to be increased. Considering such cases, the perturbation rejection mode was implemented to reject external perturbations in the position tracking task and to demonstrate the stiffen up behaviour of the robot.

The goal of the second task was to approach and establish contact with different objects. If the object property is unknown to the human operator due to lack of visual feedback or the exact position of the object is unknown because of sensory uncertainty, the robot should approach the object slowly and compliantly. While that may be true, if the robot could obtain knowledge about the object property beforehand, it can approach the object slightly faster and without the risk of breaking it by using the proper impedance. The object property detection mode, the verbal confirmation mode, and the voice control mode were used during this task to approach different objects with the proper impedance.

A. Position Tracking Task

The robot was controlled to hold the desired position with the initial impedance $\boldsymbol{K}$ set to 100N/m, and the human assistant applied an external force mainly along the x-y plane to perturb the robot. If a perturbation is detected by the proposed method, the impedance $\boldsymbol{K}$ will increase from 100N/m to 400N/m. The results of the experiment are shown in Fig. 5. The robot was first perturbed without the perturbation rejection mode activated, then the robot was perturbed again

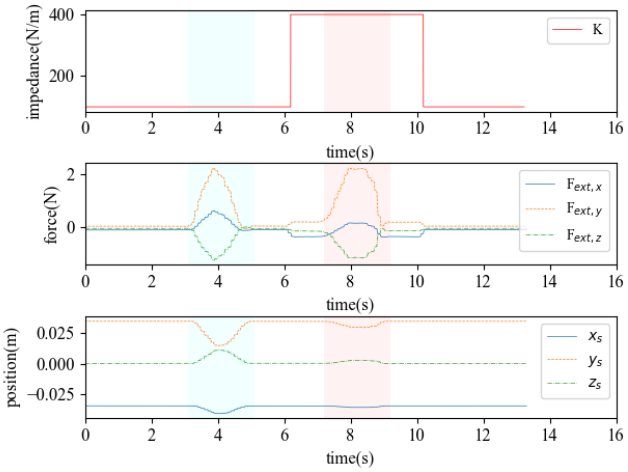

Fig. 5. Experiment results using the perturbation rejection mode (mode i) on the position tracking task. The blue shaded area shows when the robot is perturbed with the mode disabled. The red shaded area shows when the robot is perturbed with the mode activated. The first graph shows the commanded impedance $\boldsymbol{K}$. The second graph shows the external force exerted on the slave robot. The third graph shows the end-effector position of the slave robot x_s, y_s, z_s.

with approximately the same external force with the perturbation rejection mode. The displacement difference under perturbations can be seen in the third graph. The displacement of the second perturbation was much smaller than the first perturbation because the robot impedance $\boldsymbol{K}$ was set to 400 N/m as the method detects a perturbation.

B. Contact Establishing Task

In the second set of experiments, different objects were placed in front of the robot to show the proposed method changed the impedance of the robot accordingly. Then, the human operator controlled the robot to approach the object and establish contact with teleoperation. The purpose of this experiment is to demonstrate different modes of the method changing the impedance to handle different scenarios, including when the vision system performed poorly and human interventions were required. In each scenario, the robot was perturbed with approximately the same amount of force for better visual comparison on the position displacements in the figures and videos between different impedance values.

Three scenarios that requires different extents of human intervention were considered:

1) The first scenario is when the vision algorithm has good accuracy (high confidence score) and does not need human interventions. The object property detection mode was demonstrated by establishing contact with three different objects that represent metal, glass, and rubber. The results are shown in Fig. 6. The top left graph shows that the robot had an initial impedance $\boldsymbol{K}$ 100N/m, which later changed to 300N/m, 50N/m, and 200N/m by detecting metal, glass, and rubber, respectively. The bottom left graph shows that approximately 3N of external forces were applied to the robot after the impedance value changed. The effect of the impedance change could be visually interpreted by the difference in position displacements under the same amount of force showed in the yellow shaded area on the top right graph.
2) The second scenario is when the vision algorithm has poor performance and requires humans to confirm or command the correct material. The scenario was created by placing an object that is (a) made of glass but has low confidence detection result, (b) made of plastic but was identified as glass. The verbal confirmation mode was used to handle the scenario and complete the task. The robot had an initial impedance $\boldsymbol{K}$ 100N/m in both cases. In (a), the impedance changed to 50N/m after confirming the result by saying "yes"; In (b), the impedance $\boldsymbol{K}$ increased to 300N/m after overwriting the detection by saying "plastic". The demonstration videos are available in the online resource and Appendix E.
3) The third scenario is when the human operator wishes to take over the impedance control and change the impedance dynamically because the vision algorithm is performing poorly or switching discretely between predefined impedance values is no longer sufficient for the task. The scenario was created by placing an object made of plastic which the robot mistook as glass. The robot had an initial impedance value $\boldsymbol{K}$ 100N/m, and the impedance $\boldsymbol{K}$ changed to 50N/m when the robot identified the object as glass. The voice control mode was used to take over the impedance control from the robot. By activating the voice control mode, the robot impedance $\boldsymbol{K}$ was reset to 100N/m and the human operator can start adjusting the impedance value by making high and low pitch tones. The demonstration video is available in the online resource and Appendix E.

VI. Discussion

The vision-based autonomous impedance controller has the advantage of adjusting the impedance of the robot before making contact with the environment. If the environment is fragile or unstable, adjusting before contact can avoid damaging the environment or induce unstable interactions. On the other hand, some methods [14]–[17] adjust the impedance by using sensors to gather environmental information through physical interactions, which could be risky for fragile or unstable environments.

The perturbation detection mode can reject perturbation by increasing the impedance of the robot before incoming perturbations are felt. The advantage was demonstrated in the design evaluation of the perturbation rejection mode. The simulation results (see Fig. 2) show that the vision-based autonomous impedance controller has better performance in the position tracking simulation under perturbations because the controller can detect perturbations before contact and adjust the impedance beforehand.

The object property detection mode can adjust the impedance according to the detected material using visual feedback. The advantage of doing so is that the robot approaches the object with the proper impedance, which could

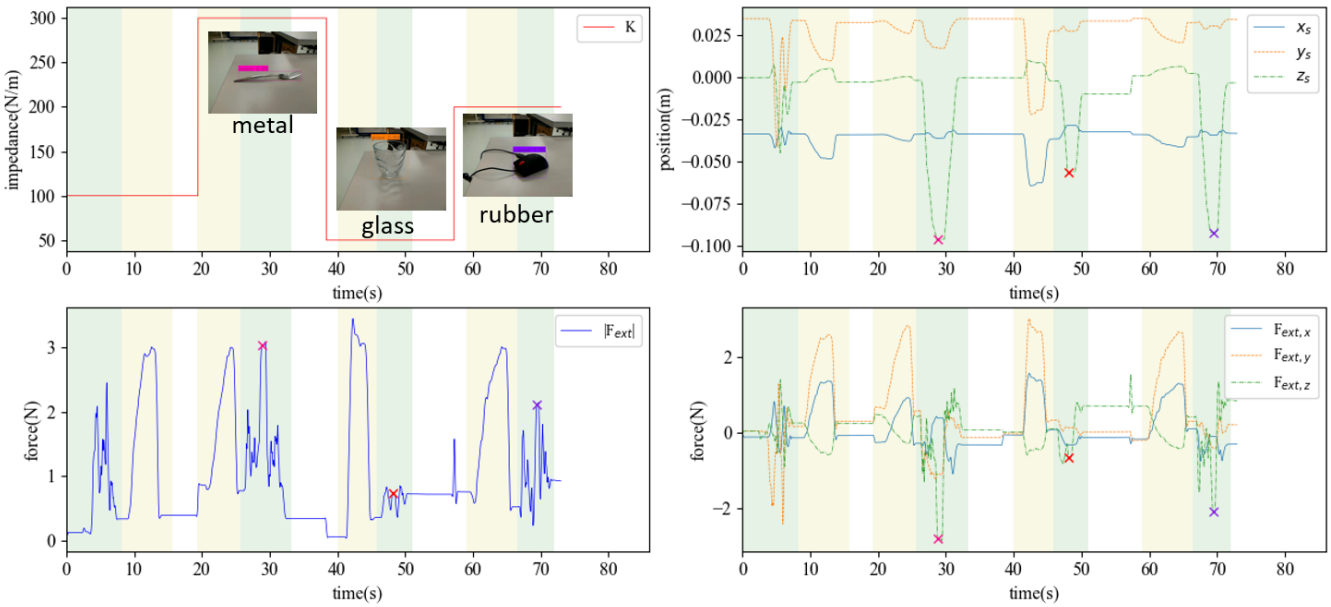

Fig. 6. Experiment results using the object property detection mode (mode ii) on the contact establishing task. The green shaded area indicates when the human operator is moving the slave robot by teleoperation. The yellow shaded area indicates when the robot is perturbed with external forces. The 'x' marker indicates the robot position and the interaction force between the robot and the object when contact is first established. The top left graph shows the impedance command, $\boldsymbol{K}$, received by the slave robot. The top right graph shows the position of the slave robot end-effector x_s, y_s, z_s. The bottom left graph shows the absolute magnitude of external force exerted on the slave robot end-effector, $\boldsymbol{F}_{ext}$. The bottom right graph shows the components of $\boldsymbol{F}_{ext}$.

lower the risk of breaking the object or induce unstable interactions.

However, there are also disadvantages to the two modes. The disadvantage of the perturbation detection mode is that the interaction forces cannot be measured so the force sensor-based methods are better suited for force tracking tasks. The disadvantages of the object property detection mode are that the detection results can sometimes have low accuracy, and the mode can only change the impedance discretely which might be insufficient if the situation requires dynamic changes in impedance.

Another advantage of the proposed method is that it can handle different environments with unexpected scenarios. This was achieved by including human interventions using the voice-based impedance control interface to interact with the vision-based autonomous impedance controller. The human operator can correct the detection results with the verbal confirmation mode when the vision algorithm is performing poorly. The voice control mode allows the human operator to take full control over the impedance when changing the impedance discretely is no longer sufficient under the task scenario.

The results of the impedance profile following task with the voice control mode show that the voice control interface can follow the desired impedance profile closely (see Fig. 3). This interface does not require physical contacts like the button interfaces [6] or other complex devices [7], [30] that require physical contact. Also, the microphone setup is much cheaper and easier to setup compared to the EMG interfaces [7], [8], [13]. The potential disadvantage of this interface is that the impedance changing speed is fixed whereas the button interface can have varied changing speed controlled by the acceleration of pressing motion. Also, prolonged production of voice signals, especially high pitch tones, may cause fatigue or discomfort faster than other interfaces that use fingers or arms because human limb muscles are generally stronger than vocal cords.

The proposed method was implemented on a teleoperation setup to validate it in real-life task scenarios. The position tracking task demonstrated the stiffening up behaviour of the robot to minimize the position displacement with the perturbation rejection mode. The contact establishing task experiment demonstrated the method adjusting the impedance under various task scenarios using different levels of autonomy within the proposed method. The results of the first scenario, where the vision is perfect, proved that the autonomous object property detection mode can adjust the impedance autonomously according to the object material (see Fig. 6). The second scenario, where the vision has poor performance, showed that the human operator can successfully interact with the vision-based autonomous impedance controller with the verbal confirmation mode when the autonomous mode is not working properly. A mutual limitation of the two modes mentioned above is that they are not able to handle scenarios if the task requires dynamic changes or small adjustments in impedance because they can only change the impedance discretely. The voice control mode tackles this limitation by allowing the human operator to take over the impedance

control fully with the voice control interface as demonstrated in the third scenario. Overall, the method was able to offload the impedance control task from the human operator with the vision-based autonomous impedance controller, as well as handling various scenarios using the voice-based impedance control interface which creates a shared control framework to keep human in the impedance control loop.

With the proposed method, the human operator can establish contact with an object using the proper impedance and reject perturbations during the approaching phase. After the contact is established, the human operator can use the voice control mode to make dynamic impedance adjustments according to the task requirements. A potential limitation of the current method is that the object property detection mode and the verbal confirmation mode would not work if the environment contains objects or scenes that are unknown to the object property detection algorithm. Although the human operator can still control the impedance with the voice control interface, it defeats the purpose of offloading the impedance control to relieve workload from the human operator.

VII. Conclusion

The scope of this study was to introduce the novel method that explores the identified research gaps and addresses the disadvantages in existing researches and further demonstrate proof-of-concept experiments on a teleoperation setup. Hence, we focused mainly on developing a novel vision-based semi-autonomous impedance control method and validated it on a teleoperation setup. In future work, we will go beyond validation experiments and conduct an in-depth human factor experiment to study whether or not the workload would decrease with the proposed method. Another interesting direction to explore would be to study the user experience of the proposed voice control interface and compare it with state-of-the-art teleimpedance interfaces, such as a button interface.

References

[1] T. Sheridan, "Telerobotics," *Automatica*, vol. 25, no. 4, pp. 487 – 507, 1989. [Online]. Available: http://www.sciencedirect.com/science/article/pii/0005109889900939

[2] N. Hogan, "Adaptive control of mechanical impedance by coactivation of antagonist muscles," *IEEE Transactions on Automatic Control*, vol. 29, no. 8, pp. 681–690, August 1984.

[3] J. McIntyre, F. A. Mussa-Ivaldi, and E. Bizzi, "The control of stable postures in the multijoint arm," *Experimental Brain Research*, vol. 110, pp. 248–264, 1996.

[4] A. Ajoudani, S. Godfrey, N. Tsagarakis, and A. Bicchi, *Teleimpedance Control: Overview and Application*, 02 2016, pp. 151–169.

[5] D. Walker, "Design of versatile telerobotic systems using variable impedance actuation and control," Ph.D. dissertation, 06 2013.

[6] L. Peternel, T. Petric, and J. Babič, "Robotic assembly solution by human-in-the-loop teaching method based on real-time stiffness modulation," *Autonomous Robots*, vol. 42, pp. 1–17, 04 2017.

[7] A. Ajoudani, N. Tsagarakis, and A. Bicchi, "Tele-impedance: Teleoperation with impedance regulation using a body–machine interface," *The International Journal of Robotics Research*, vol. 31, no. 13, pp. 1642–1656, 2012. [Online]. Available: https://doi.org/10.1177/0278364912464668

[8] L. Peternel, T. Petric, E. Oztop, and J. Babič, "Teaching robots to cooperate with humans in dynamic manipulation tasks based on multi-modal human-in-the-loop approach," *Autonomous Robots*, vol. 36, pp. 1–14, 01 2014.

[9] A. Ajoudani, C. Fang, N. Tsagarakis, and A. Bicchi, "Reduced-complexity representation of the human arm active endpoint stiffness for supervisory control of remote manipulation," *The International Journal of Robotics Research*, vol. 37, 11 2017.

[10] J. Buchli, E. Theodorou, F. Stulp, and S. Schaal, "Variable impedance control a reinforcement learning approach," 07 2010.

[11] K. Kronander and A. Billard, "Online learning of varying stiffness through physical human-robot interaction," *Proceedings - IEEE International Conference on Robotics and Automation*, pp. 1842–1849, 05 2012.

[12] P. Kormushev, S. Calinon, and D. Caldwell, "Imitation learning of positional and force skills demonstrated via kinesthetic teaching and haptic input," *Advanced Robotics*, vol. 25, 03 2011.

[13] C. Yang, C. Zeng, C. Fang, W. He, and Z. Li, "A dmps-based framework for robot learning and generalization of humanlike variable impedance skills," *IEEE/ASME Transactions on Mechatronics*, vol. 23, no. 3, pp. 1193–1203, June 2018.

[14] C. Yang, G. Ganesh, S. Haddadin, S. Parusel, A. Albu-Schaeffer, and E. Burdet, "Human-like adaptation of force and impedance in stable and unstable interactions," *IEEE Transactions on Robotics*, vol. 27, no. 5, pp. 918–930, Oct 2011.

[15] A. Brygo, I. Sarakoglou, N. Tsagarakis, and D. G. Caldwell, "Tele-manipulation with a humanoid robot under autonomous joint impedance regulation and vibrotactile balancing feedback," in *2014 IEEE-RAS International Conference on Humanoid Robots*, Nov 2014, pp. 862–867.

[16] L. Muratore, A. Laurenzi, E. M. Hoffman, L. Baccelliere, N. Kashiri, D. G. Caldwell, and N. G. Tsagarakis, "Enhanced tele-interaction in unknown environments using semi-autonomous motion and impedance regulation principles," in *2018 IEEE International Conference on Robotics and Automation (ICRA)*, May 2018, pp. 5813–5820.

[17] P. Balatti, D. Kanoulas, N. Tsagarakis, and A. Ajoudani, "A method for autonomous robotic manipulation through exploratory interactions with uncertain environments," *Autonomous Robots*, Aug. 2020. [Online]. Available: https://doi.org/10.1007/s10514-020-09933-w

[18] L. Peternel and J. Babic, "Humanoid robot posture-control learning in real-time based on human sensorimotor learning ability," 05 2013, pp. 5329–5334.

[19] M. A. Zamani and E. Oztop, "Simultaneous human-robot adaptation for effective skill transfer," in *2015 International Conference on Advanced Robotics (ICAR)*, July 2015, pp. 78–84.

[20] L. Peternel, E. Oztop, and J. Babič, "A shared control method for online human-in-the-loop robot learning based on locally weighted regression," in *2016 IEEE/RSJ International Conference on Intelligent Robots and Systems (IROS)*, Oct 2016, pp. 3900–3906.

[21] J. Kofman, Xianghai Wu, T. J. Luu, and S. Verma, "Teleoperation of a robot manipulator using a vision-based human-robot interface," *IEEE Transactions on Industrial Electronics*, vol. 52, no. 5, pp. 1206–1219, Oct 2005.

[22] A. Dragan and S. Srinivasa, "A policy-blending formalism for shared control," *The International Journal of Robotics Research*, vol. 32, pp. 790–805, 06 2013.

[23] E. You and K. Hauser, "Assisted teleoperation strategies for aggressively controlling a robot arm with 2d input," 06 2011.

[24] N. Amirshirzad, A. Kumru, and E. Oztop, "Human adaptation to human–robot shared control," *IEEE Transactions on Human-Machine Systems*, vol. 49, no. 2, pp. 126–136, April 2019.

[25] A. Albu-Schaffer, C. Ott, U. Frese, and G. Hirzinger, "Cartesian impedance control of redundant robots: recent results with the dlr-light-weight-arms," in *2003 IEEE International Conference on Robotics and Automation (Cat. No.03CH37422)*, vol. 3, Sep. 2003, pp. 3704–3709 vol.3.

[26] M. W. Spong, "Modeling and Control of Elastic Joint Robots," *Journal of Dynamic Systems, Measurement, and Control*, vol. 109, no. 4, pp. 310–318, 12 1987. [Online]. Available: https://doi.org/10.1115/1.3143860

[27] L. Sharan, R. Rosenholtz, and E. Adelson, "Material perception: What can you see in a brief glance?" *Journal of Vision - J VISION*, vol. 9, pp. 784–784, 08 2010.

[28] S. Bell, P. Upchurch, N. Snavely, and K. Bala, "Material recognition in the wild with the materials in context database," 06 2015, pp. 3479–3487.

[29] J. Redmon and A. Farhadi, "Yolov3: An incremental improvement," *arXiv*, 2018.

[30] D. S. Walker, R. P. Wilson, and G. Niemeyer, "User-controlled variable impedance teleoperation," in *2010 IEEE International Conference on Robotics and Automation*, 2010, pp. 5352–5357.

A

Experiment Setup

The technical details of the teleoperation setup are elaborated in this chapter. The hardware setup for the teleoperation motion control is introduced in section A.1, the vision system is introduced in section A.2.

A.1. Teleoperation hardware setup

The slave robot is a Force Dimension Sigma.7 haptic device, the specifications can be found on the Force Dimension company website [5]. The master device is a computer mouse so there is no force feedback in this teleoperation setup. The master device and the slave robot communicates through local user datagram protocol (UDP) ports.

The motion command is generated by the planar motion of the mouse which is captured by tracking the cursor movement on a window (See Fig. A.1). The motion command is used to control the y-z plane motion of the slave robot.

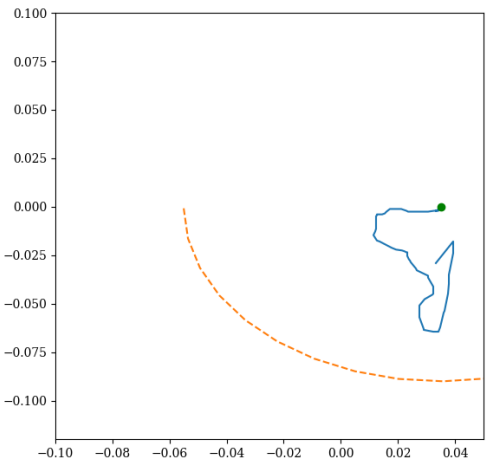

Figure A.1: Motion control window for tracking the cursor position. The green dot represent the starting robot position. The orange dashed line represents the safe work space. The blue line is the robot path.

The robot receives the commands and realizes them in a C++ framework that came with the Force Dimension haptic SDK. A simple visualization of the motion control loop and the corresponding hardware is shown in Fig. A.2.

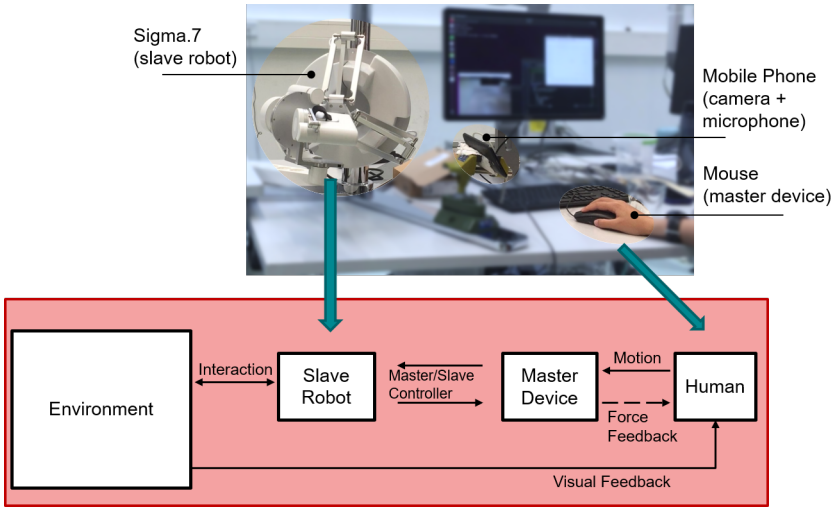

Figure A.2: Teleoperation motion control loop

A.2. Vision system setup

The impedance command of the robot is given according to the output of the algorithms. The impedance command is realized on the slave robot through the Cartesian impedance control method.

The vision system uses an Asus Zenfone 2 with the DroidCam application installed and connected to the PC with an USB cable that also has a DroidCam PC interface installed[3]. This allows the PC to access the microphone and camera of the phone.

The perturbation rejection mode uses a motion detection algorithm and a tracking algorithm to detect perturbations (see Fig. A.3a). The motion is detected by calculating the first video frame (static background) with the current video frame, and then bound the difference between the two frames with a rectangle. The robot tracking is done with the OpenCV built-in object tracker, the CSRT tracker was chosen because the performance seems to be more optimal comparing to other types of trackers. The perturbation will be detected when the motion bounding rectangle and the centroid of the tracker are less than a safe distance set by the user depending on how careful they wish to be.

The object property detection mode uses a pre-trained object detection algorithm (YOLOv3) [8] with the output results that are changed from objects into materials to demonstrate the autonomous changing of impedance (see Fig. A.3b).

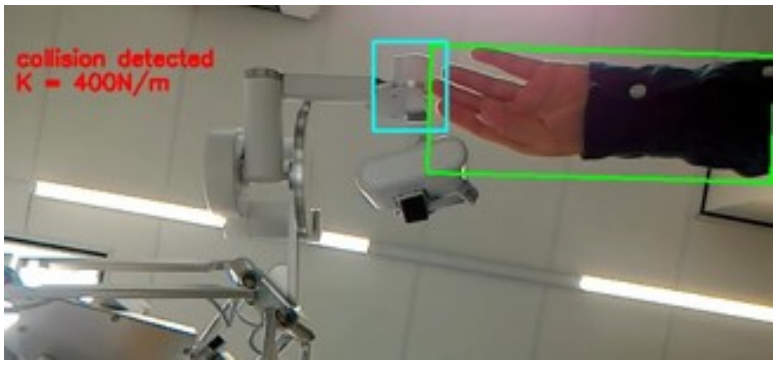

(a) Detection algorithm Implementation by combing the tracking algorithm (box on the left) and the motion detection algorithm (box on the right).

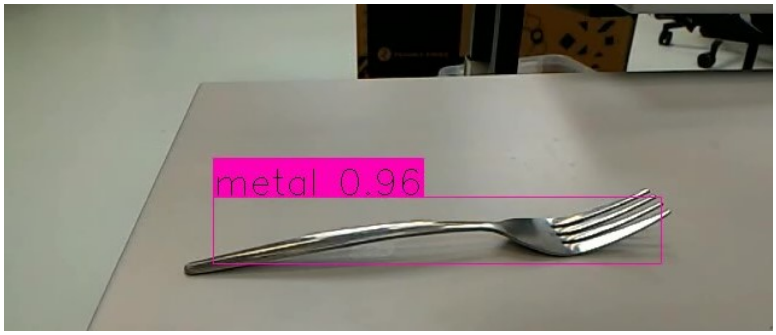

(b) Object detection algorithm output displaying the detected materials and its confidence score.

Figure A.3: Implementation of the vision algorithms in the vision-based impedance controller.

B

Controller Comparison Simulation

A detailed explanation of the simulation in the design evaluation of the perturbation rejection mode (mode i). The simulation was considered to be only in one dimension for simplicity and was carried out in MATLAB.

B.1. Object and robot arm collision simulation

The parameters used in this simulation are listed in table B.1.

Table B.1: THE PARAMETERS OF THE OBJECT COLLISION SIMULATION

Symbol	Property	Quantity
m_1	incoming object mass	2 kg
v_1	object initial velocity	5 m/s
m_2	robot mass	10 kg
v_2	robot initial velocity	0 m/s
k	robot initial stiffness	100 N/m
c	robot initial damping coefficient $(2 * 0.7 * \sqrt{(k)})$	14 Ns/m
M	total mass $(m_1 + m_2)$	12 kg
v_f	velocity after collision	0.6667 m/s

An object with an initial speed of 5 m/s collides with the robot that is holding the desired position in a position tracking task as shown in Fig. B.1. The collision is assumed to be a non-elastic collision e=0 so the final velocity of the robot and the object can be derived from the conservation of the momentum:

$$m_1 v_1 + m_2 v_2 = (m_1 + m_2) v_f = M v_f \tag{B.1}$$

$$v_f = \frac{m_1 v_1}{M} \tag{B.2}$$

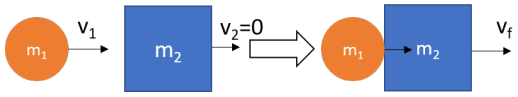

Figure B.1: the object (orange) colliding with the robot (blue)

After the collision, the robot and the object are attached and moving with the velocity of v_f. The reaction force of the robot is generated as follow since the robot is under impedance control:

$$F = -kx - c\dot{x} \tag{B.3}$$

where x is the position displacement of the robot.
The situation is equivalent to a spring-mass-damper system so the position of the robot is derived by solving the differential equation (eq. B.4) using the ode function in MATLAB.

$$M\ddot{x} + c\dot{x} + kx = 0 \tag{B.4}$$

where x is the robot position.

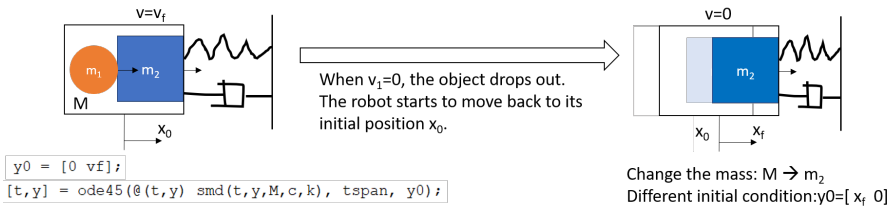

Figure B.2: The equivalent spring-mass-damper system before and after the object detached from the robot.

The equivalent spring-mass-damper system when the object and the robot are attached has a mass of M, and when the object drops out, the spring-mass-damper system only has the mass of the robot m_2 as shown in Fig. B.2. For the sake of completeness, the simulation starts from the object colliding with the robot until the robot goes back to its equilibrium position (initial position). However, only the maximum position displacement was considered when evaluating the performance of the controllers because the human operator is likely to react through the master device after the object drops out. Hence, the results are zoomed in around the maximum displacement.

The impedance commands of the controllers during the collision simulation are shown in Fig. B.3. The vision-based controller has a slight time advantage over the other position sensor-based controllers which results in better performance when rejecting the perturbation.

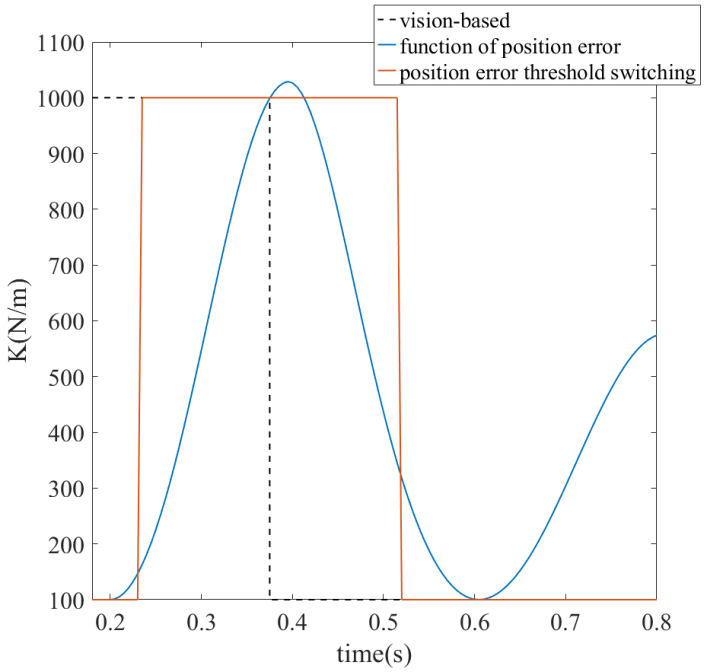

Figure B.3: The controllers impedance command versus time plot under object collision perturbation

B.2. Impact force simulation

The parameters used in this simulation are listed in table B.2.

Table B.2: THE PARAMETERS OF THE IMPACT FORCE SIMULATION

Symbol	Property	Quantity
m	robot mass	10 kg
v	robot initial velocity	0 m/s
k	robot initial stiffness	100 N/m
c	robot initial damping coefficient $(2 * 0.7 * \sqrt{(}k))$	14 Ns/m
F_{ext}	impact force	See Fig. B.4

The robot is under impedance control same as the object collision simulation. The system can be viewed as a spring-mass-damper system and the robot position is also obtained by solving the differential function. The difference is that an external force is exerted on the spring-mass-damper system to induce impact force perturbation.

$$M\ddot{x} + c\dot{x} + kx = F_{ext}$$

where x is the robot position. F_{ext} is the impact force perturbation.

The impact force was simulated with an impact time of 200 ms which is within the average reaction time for humans [1]. We can assume that the human operator is not likely to react during the sudden impact force perturbation as shown in Fig. B.4. Additionally, for the same reasoning mentioned in the object collision simulation section that the human operator might react after the perturbation is over, we focused only on the maximum position displacement.

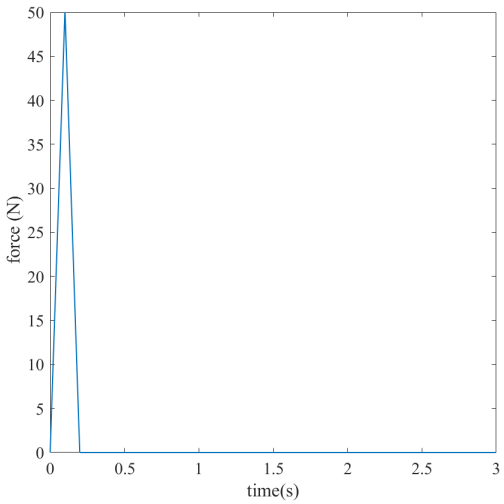

Figure B.4: The simulated impact force versus time figure.

The impedance commands of the controllers are shown in Fig. B.5. The vision-based controller has a slight time advantage over the other force sensor-based controllers which results in better performance in rejecting the perturbation.

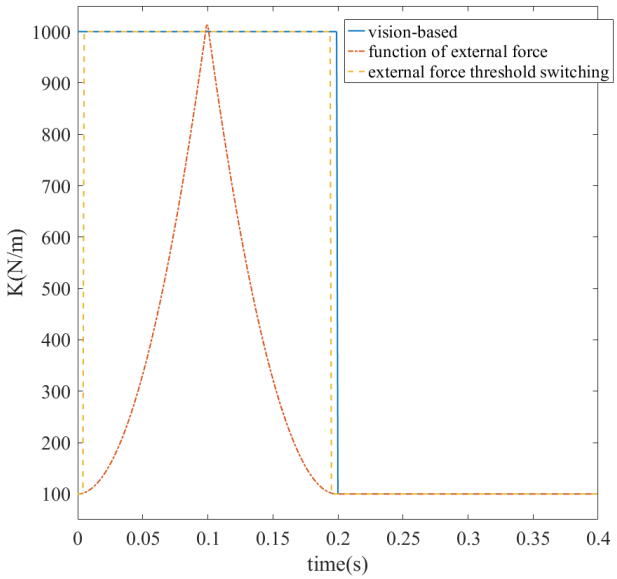

Figure B.5: The controllers impedance command versus time plot under impact force perturbation.

C

Mechanical Properties of the Chosen Materials

In order to implement the object property detection mode (mode ii), the relation between the object property and the impedance was explored. The data was collected mainly from the "Material Data Book" from the Cambridge Engineering Sector [2] along with some extra resources [4][6][9][7] to supplement the data for certain materials.

The categorization is based on the elasticity and the fragility of the material. The elasticity is defined based on the Young's Modulus E of the material. The material is considered rigid if E is larger than 0.5 GPa, and elastic if E is less than or equal to 0.5 GPa. The fragility is related to the Yield Strength σ_y or Tensile Strength σ_{ts}(for materials stronger in compression such as glass, ceramic, stone, concrete, and paper), and the Fracture Toughness K_{IC} which is a quantitative way of expressing a material's resistance to crack propagation. The material is considered not fragile if the material is elastic or σ_y/σ_{ts} is larger than 10 MPa and K_{IC} is larger than or equal to 1 MPa·m$^{1/2}$. Otherwise, the material is considered fragile. The chosen materials are categorized into three groups: "Elastic, Not Fragile", "Rigid, Not Fragile", and "Rigid, Fragile". The results are shown in table. C.1.

Three impedance values are assigned to the groups in order to demonstrate the autonomous impedance changing behaviour. The actual optimal impedance to interact with the materials in each group still needs to be determined through experiment. However, this is not the main focus of this study so the assigned impedance values will suffice for the study.

Material	type	Young's Modulus(GPa)	Average	Rigid/Elastic	Yield Strength/ Tensile Strength(MPa)	Compressive Strength(MPa)	Fracture Toughness (MPa√m)	Fragility
Glasses	soda-lime	68-72	70.000	Rigid	31-35	360-420	0.55-0.7	Fragile
Leather		0.1-0.5	0.300	Elastic	5-10		3-5	Not Fragile
Metal	Stainless Steels	189-210	199.500	Rigid	170-1000		62-280	Not Fragile
	Aluminium Alloys	68-82	75.000	Rigid	30-500		22-35	Not Fragile
	Copper Alloys	112-148	130.000	Rigid	30-500		35-90	Not Fragile
Paper	(per fiber)	0-10	5.000	Rigid	15-20 (a sheet)			Fragile
Plastic	ABS	1.1-2.9	2.000	Rigid	18.5-51		1.19-4.3	Not Fragile
	PVC	2.14-4.14	3.140	Rigid	35.4-52.1		1.46-5.12	Not Fragile
	Polypropylene(PP)	0.896 - 1.55	1.223	Rigid	20.7 - 37.2	34.5-55.2	3 - 4.5	Not Fragile
Concrete		25-38	31.500	Rigid	2-7	32-60	0.35-0.45	Fragile
Stone		6.9-21	13.950	Rigid	5-17	34-248	0.7-1.5	Not Fragile
Wood	along grain	6-20	13.000	Rigid	30-70	60-100	5-9	Not Fragile
	transverse	0.5-3	1.750	Rigid	2-6	40-65	0.5-0.8	Fragile
Ceramic	Alumina	215-413	314.000	Rigid	350-665	690-5500	3.3-4.8	Not Fragile
	Silicon Nitride	280-310	295.000	Rigid	690-800	524-5500	4-6	Not Fragile
	Porcelain	48-69	58.500	Rigid	7-10	172-344	1.9-2.1	Fragile
Elastomer	Butyl Rubber	0.001-0.002	0.002	Elastic	2-3		0.07-0.1	Not Fragile
(rubber)	Natural Rubber	0.0015-0.0025	0.002	Elastic	20-30		0.15-0.25	Not Fragile

Figure C.1: Raw data and categorization of the chosen materials. The categorization results are shaded in different color for better visualization. The tensile strength values are written in blue to distinguish from the yield strength.

D

Voice control GUI design

A GUI (graphic user interface) was designed for the evaluation experiment of the voice control mode. The GUI allows easy access to the voice control interface. It is designed with the intention to conduct a human factor experiment on the voice control interface. Although in this master thesis the interface was only used on one user for the design evaluation of the voice control mode.

For the sake of future possibilities in exploring the user experience of this interface, a thorough explanation of the interface design is included here:
The user can set the current phase to "practice" or "task" depending on which trial he/she is currently in. The recorded data will only be saved during the task phase when the user presses the "Stop" button. Additionally, the user can set the threshold frequency f_{th} (default is 300 Hz) by entering the number in Hz since female and male have different range of voice frequency.

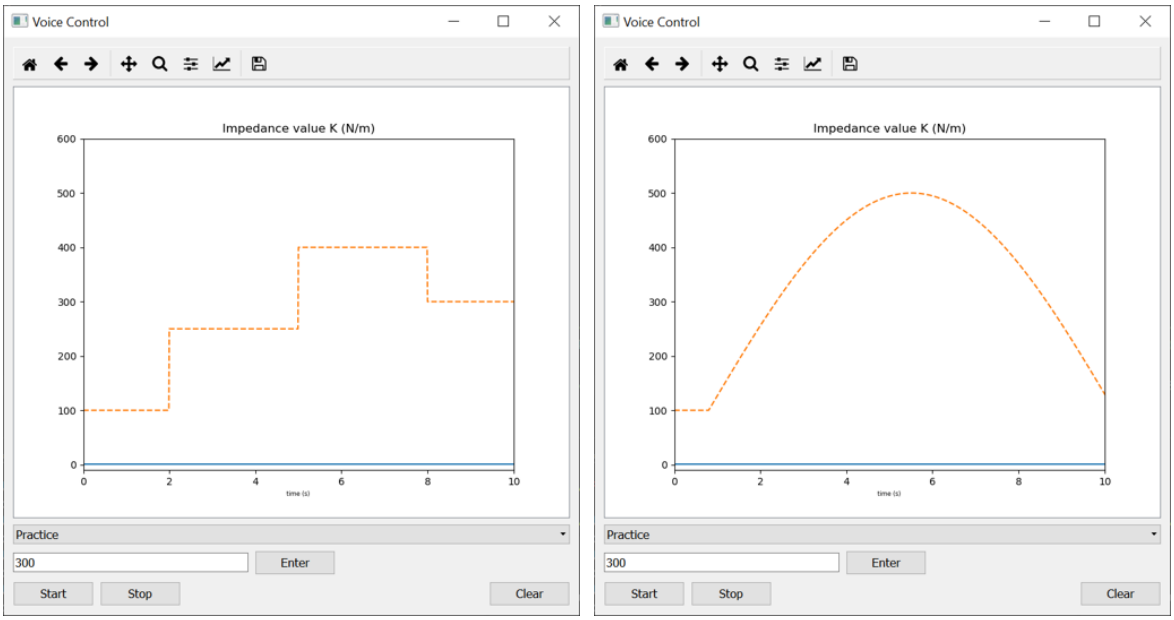

(a) step change (b) sine wave

Figure D.1: The GUI with two different desired impedance profiles.

The videos of the evaluation experiment where a user is trying to follow the desired impedance profiles with the voice control interface is available at:
(a) step change: `https://youtu.be/bZfjJkvtbZw`
(b) sine wave: `https://youtu.be/vcTUFGrB2YM`.

E

Proof-of-concept Experiment Results

This chapter contains the results of the proof-of-concept experiments. The plots are shown in the first section and the video links of the experiments are listed in the second section.

E.1. Results of the proof-of-concept experiments

As mentioned in the main context, the impedance matrix $\boldsymbol{K}$ has no rotation with respect to the robot base frame, and the proposed method commands the same value for all three axes in Cartesian space. Therefore, the impedance matrix $\boldsymbol{K}$ will be described in a single value and plotted with one value in graphs.

The force data collected during experiments were noisy which we assumed were generated from the robot hardware. To make the plot clear, all the force data plotted in the following figures were filtered with a lowpass filter which has a cutoff frequency of 3 Hz. The cutoff frequency was chosen by analyzing the collected force data with fast Fourier transform.

The result of the proof-of-concept experiment for the perturbation rejection mode (mode i) is shown in Fig. E.1. The robot is perturbed with approximately the same amount of external force with and without the perturbation rejection mode activated.

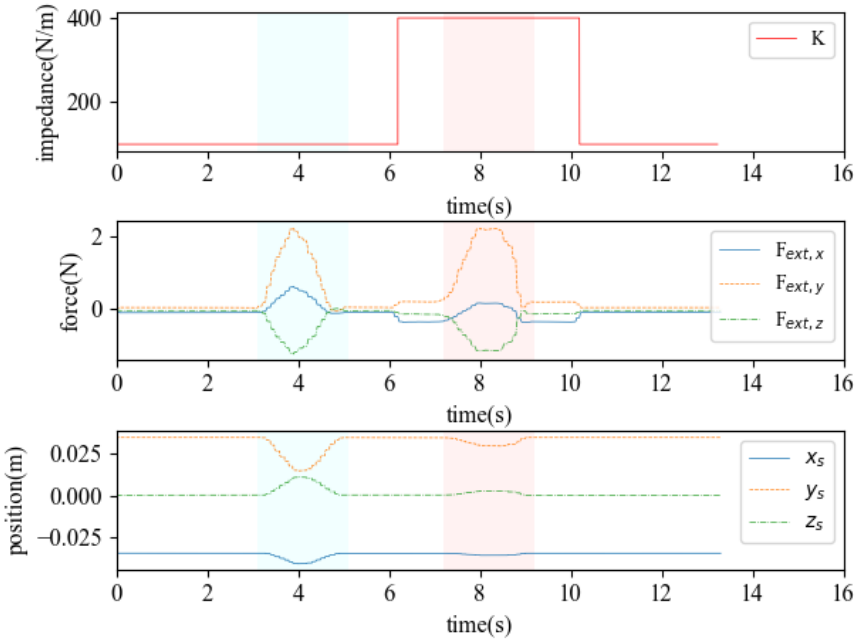

Figure E.1: The experiment result of the perturbation rejection mode. The blue shared area indicates when the robot is perturbed without the perturbation rejection mode activated. The red shaded area indicates when the robot is perturbed with the perturbation rejection mode activated. The top graph is the impedance command $\boldsymbol{K}$. The middle graph is the components of the external force exerted on the robot $\boldsymbol{F}_{ext}$. The bottom graph is the position of the robot x_s y_s z_s.

The following experiment results are all plotted in the same format which is four subplots: The top left graph shows the impedance command K sent to the robot; the top right figure shows the position of the robot, x_s, y_s, and z_s; the bottom left graph shows the absolute magnitude of the external force exerted on the robot, $\boldsymbol{F}_{ext}$. The bottom right graph shows the components of $\boldsymbol{F}_{ext}$.

The result of the proof-of-concept experiment for the object property detection mode (mode ii) is shown in Fig. E.2. Three objects that the object detection algorithm detects as metal, glass, and rubber were placed in front of the vision system. The robot changed the impedance accordingly and approximately 3N of external force was exerted to validate that the impedance was realized on the robot.

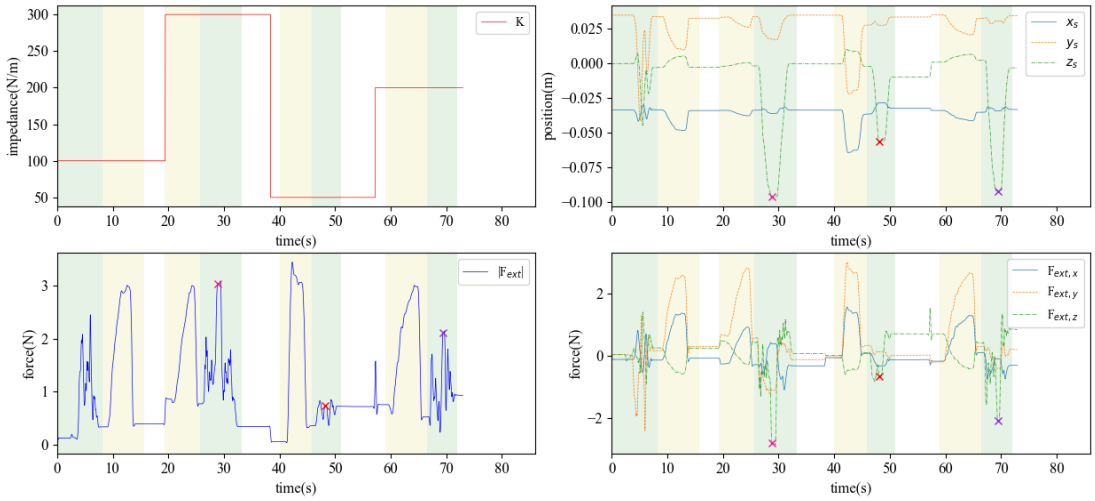

Figure E.2: The experiment results of the object property detection mode. The green shaded area indicates when the human operator is teleoperating the robot. The yellow shaded area is when the robot is under perturbation. The 'x' marker indicates the robot position and the interaction force between the robot and the object when contact is first established.

The results of the proof-of-concept experiment for the verbal confirmation mode (mode iii). Two objects were placed in front of the vision system where one is correctly detected and the other detection was incorrect. The result of the correct detection scenario is shown in Fig. E.3a where the human operator confirmed the detection result by saying "yes" to the microphone. The result of the incorrect detection scenario is shown in Fig. E.3b where the human operator overwrites the detection result by saying "plastic" to the microphone.

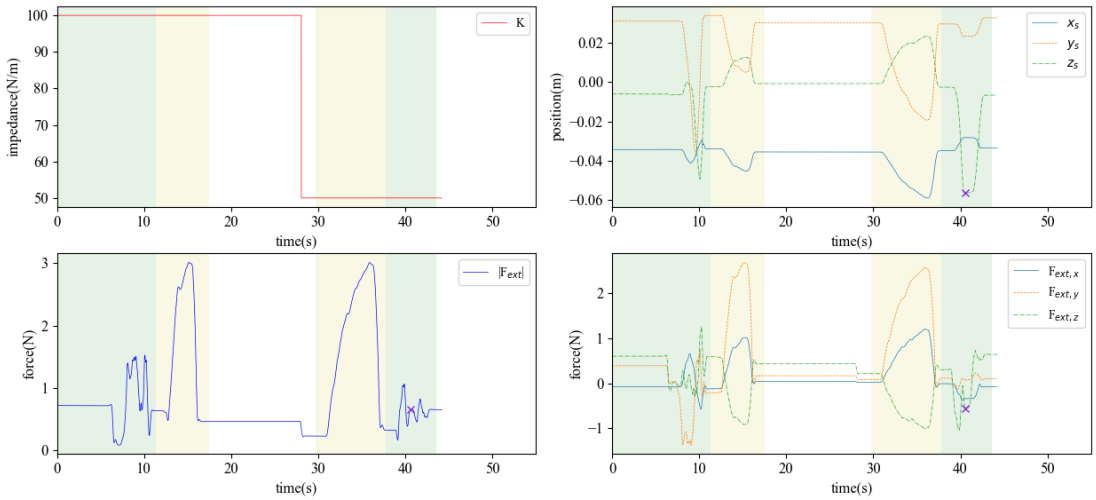

(a) The experiment results of the verbal confirmation mode under correct detection scenario.

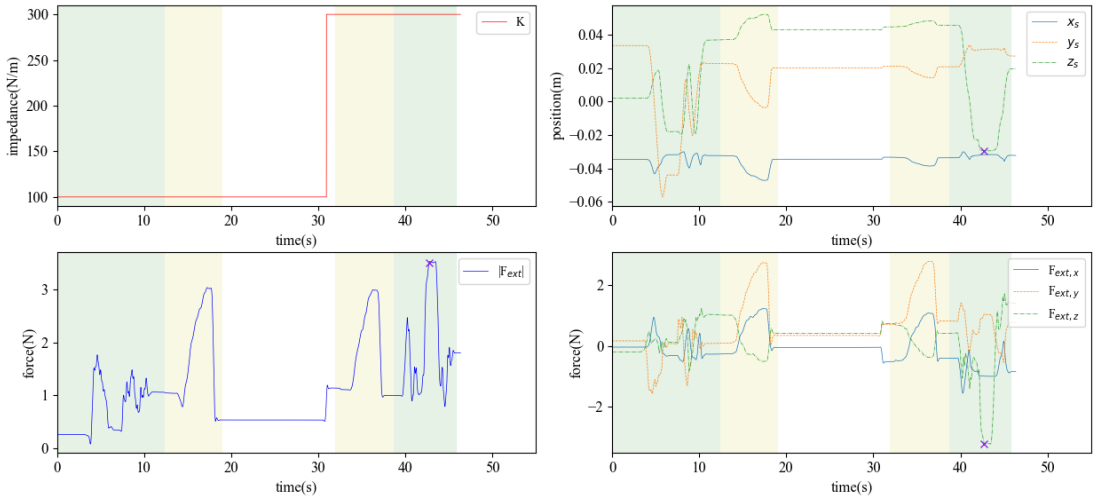

(b) The experiment results of the verbal confirmation mode under incorrect detection scenario.

Figure E.3: Results of the experiments using the verbal confirmation mode. The green shaded area indicates when the human operator is teleoperating the robot. The yellow shaded area is when the robot is under perturbation. The 'x' marker indicates the robot position and the interaction force between the robot and the object when contact is first established.

The result of the proof-of-concept experiment for the voice control mode (mode iv) is shown in Fig. E.4. An object was placed in front of the vision system where the robot automatically adjusts the impedance. However, the human operator wished to change the impedance as they assess the situation. The voice control interface was activated when the time is around 32s where the impedance resets to 100 N/m and the human operator took over the impedance control.

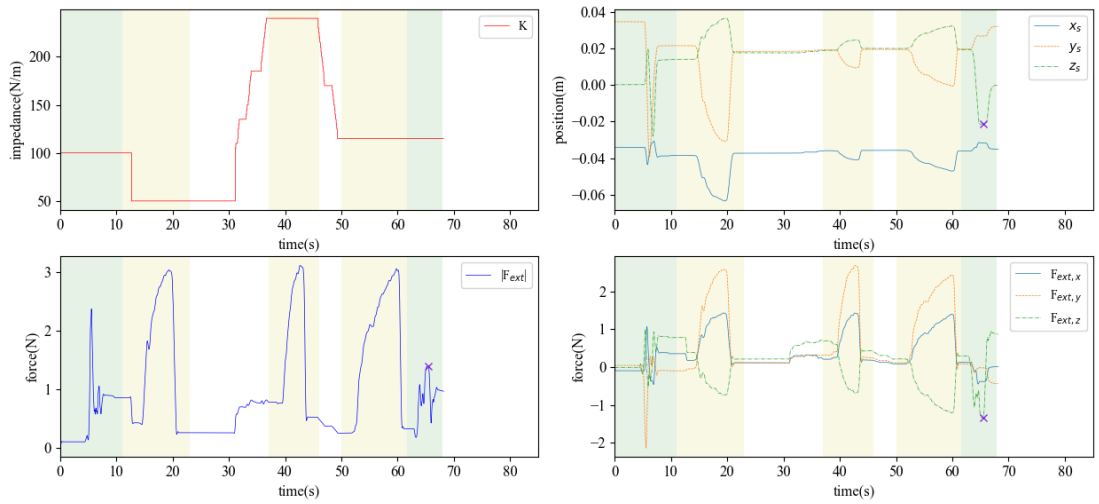

Figure E.4: Results of the experiments using the voice control mode. The green shaded area indicates when the human operator is teleoperating the robot. The yellow shaded area is when the robot is under perturbation. The 'x' marker indicates the robot position and the interaction force between the robot and the object when contact is first established.

E.2. Online video resource listings

1. **Perturbation Rejection Mode**:
   A video showing the robot being perturbed with approximately 3N of external force with and without the perturbation rejection mode is available at:
   `https://youtu.be/Ic4oGVHgjbA`.

2. **Object Property Detection Mode**:
   A video showing the robot adjusting the impedance according to the detected material while the human assistant perturbs the robot with approximately 3N of external force is available at:
   `https://youtu.be/EIz4RqWDxEc`.

3. **Verbal Confirmation Mode**:
   Correct detection scenario: A video showing the human confirming the detection result by saying "yes" is available at:
   `https://youtu.be/QhzELui8RuE`.
   Incorrect detection scenario: A video showing the human overwriting the detection result by saying "plastic" is available at:
   `https://youtu.be/9aouEGbxdM8`.

4. **Voice Control Mode**:
   A video showing the human operator controlling the robot impedance with the voice control interface is available at:
   `https://youtu.be/oV4HbYZ8P7U`.

Reference

[1] R. Abbasi-Kesbi, H. Memarzadeh-Tehran, and M. J. Deen. Technique to estimate human reaction time based on visual perception. *Healthcare Technology Letters*, 4(2):73–77, 2017.

[2] Cambridge University Engineering Department. *Materials Data Book*. 2003.

[3] Dev47apps. Droidcam. URL `https://www.dev47apps.com/droidcam/linux/`.

[4] Nick Engler. The nature of wood: Wood strength. URL `http://workshopcompanion.com/KnowHow/Design/Nature_of_Wood/3_Wood_Strength/3_Wood_Strength.htm`.

[5] force dimension. Sigma.7 specifications. URL `https://www.forcedimension.com/products/sigma-7/specifications`.

[6] Andrew Ivankin, V.G. Sanaev, Galina Gorbacheva, A.K. Ageev, D. Kiryukhin, G. Kichigina, and P.P. Kushch. Modification of properties of natural cellulose- containing composite materials by fluoroelastomers and tetrafluoroethylene telomers. *Bulletin of Higher Educational Institutions. Lesnoi Zhurnal (Forestry journal)*, pages 122–132, 03 2018. doi: 10.17238/issn0536-1036.2018.2.122.

[7] Iron Boar Labs Ltd. Makeitfrom.com. URL `https://www.makeitfrom.com/compare/Alumina-Aluminum-Oxide-Al2O3/Engineering-Porcelain`.

[8] Joseph Redmon and Ali Farhadi. Yolov3: An incremental improvement. *arXiv*, 2018.

[9] dr. ir. R.H.J. Peerlings R.W. Koppelaar, ir. L.A.A. Beex. Properties of paper - the mechanical behavior of single paper fibers. 07 2009.